Theoretical Investigation of Natural Convection Heat Transfer Through Rectangular Enclosure

دراسه نظريه لإنتقال الحرارة بالحمل الحر خلال كهف مستطيل

Amro M. Abou Elenein *, Ahmed A. Sultan *, Hesham M. Mostafa **
and Ahmed A. Hegazi *.
*Egypt Mansoura, Mansoura University, Mech. Power Eng. Dept .
** Egypt, Tenth of Ramadan City, Higher Technological Institute, Mech. Power Eng. Dept .

ملخص البحث

فى هذا البحث تم عمل دراسة نظرية لإنتقال الحرارة بالحمل الحر خلال كهف مستطيل مملؤ بموائع الماء أو الهواء حيث يتم تسخين الجدار السفلى بفيض حرارى ثابت والجدران الرأسيه معزوله ويتم تبريد الجدار العلوي. تمت الدراسة العددية بفرض أن المائع مستقر وثنائي الأبعاد حيث تم حل المعادلات الحاكمة للكتلة وكمية الحركة وانتقال الطاقة باستخدام تقنيه الفرق المحدود. تم تنفيذ المحاكاة لعدة قيم من نسبة العرض إلى الارتفاع بنسب تتراوح ما بين 0.66 إلى 8 وأيضاً عدد رايلى على أساس الأرتفاع والذي يتراوح قيمته مابين 10^3 إلى 10^6. تم تحليل ومناقشة توزيع درجات الحرارة وكذلك إنتقال الحرارة خلال الكهف. تمت مقارنة نتائج انتقال الحرارة بنتائج انتقال الحرارة من الأبحاث السابقة وذلك للوقوف على مدى التقارب بينهما. أوضحت النتائج أن معدل إنتقال الحرارة يزيد مع زيادة عدد رايلى وأيضاً يزيد مع زيادة النسبة بين العرض للإرتفاع حتى 2 ثم يثبت مع زيادة هذة النسبه. تم الحصول على معادلة تربط العلاقة بين إنتقال الحرارة وعدد رايلى والنسبة بين العرض للإرتفاع لكل من الهواء والماء.

ABSTRACT

Theoretical investigations on natural convection heat transfer have been carried out inside rectangular enclosures filled with air or water. Heat transfer and fluid flow due to buoyancy forces in an enclosure are achieved. The vertical walls are insulated while the top wall is cooled and the bottom wall is heated under uniform heat flux. Steady laminar natural convection in air or water-filled, 2-D rectangular enclosure is studied numerically. The finite difference technique is used to solve the mass, momentum and energy transfer governing equations. The computational results are presented in the form of isotherm and streamline plots. Simulations are performed for several values of both the width-to-height aspect ratio of the enclosure in the range between 0.66 and 8, and the modified Rayleigh number based on the enclosure height in the range between 10^3 and 10^6, whose influences upon the flow patterns, the temperature distributions, and the heat transfer rate are analyzed and discussed. The heat transfer rate from heated enclosure increases as the aspect ratio (A) increases until A=2 and then remains constant with further increase in aspect ratio. The heat transfer rate increases as the modified Rayleigh number increases. Nusselt numbers for both air or water filled enclosures are correlated with both aspect ratio (A) and modified Rayleigh number (Ra^*). In order to validate the numerical code for the present study, present results have been compared with the benchmark results of previous researches.

Key words: Natural convection, Heat transfer, Rectangular enclosure, Numerical analysis.

1. INTRODUCTION

Natural convection in enclosures has been extensively studied both experimentally and numerically, being of considerable interest in many engineering and scientefic applications such as collection of solar energy, operation and safety of nuclear reactors, energy efficient design of buildings, effective cooling of electronic components and

machinery. Most of the papers in this field are substantially oriented toward the study of rectangular enclosures where the heat flow is typically unidirectional, i.e., the buoyancy is induced by imposing a heating either from the side (for conventional convection) or from below (for thermal instabilities) Catton [1] and Ostrach [2]. Ciofalo and Karayiannis [3] and Chinnokotla et al. [4] studied the case of enclosures having non-simple geometries. Mixed temperature and heat flux conditions on the same boundary wall were studied by November and Nansteel [5] and Valencia and Frederick [6]. Studies on natural convection in rectangular enclosures heated from below and cooled along a single side or both sides have been carried out respectively by Anderson and Lauriat [7] and by Ganzarolli and Milanez [8]. More recently the case of heating from one side and cooling from the top has been analyzed by Aydin et al. [9-10] who investigated both the effects of Prandtl number upon heat and momentum transfer inside square cavities and the influence of the aspect ratio for air-filled, rectangular enclosures. Shati et al. [11] performed an empirical solution for the case of radiation and natural convection in square and rectangular enclosures and also provided a correlation equation to calculate the total Nusselt number for these cases.

The aim of the present paper is to investigate natural convection in rectangular enclosures heated from below and cooled from above with adiabatic condition at the sidewalls. The study is conducted numerically under the assumption of steady laminar, two dimensional flow for different values of both the width-to-height aspect ratio of the enclosure in the range between 0.66 and 8, and the modified Rayleigh number based on the enclosure height in the range between 10^3 and 10^6, whose influence upon the flow patterns, the temperature distributions and the heat transfer rates are analyzed and discussed for air or water-filled enclosures.

Nomenclature

A aspect ratio, (L/H)
Cp specific heat at constant pressure (J/kgk)
g gravitational acceleration (m/s^2)
H height of the enclosure (m)
h convective heat transfer coefficient (W/m^2K)
k_f thermal conductivity of the fluid (W/mK)
L width of the enclosure (m)
Nu Nusselt number, (hL/k_f)
P pressure (Pa)
Pr Prandtl number, (ν/α)
q" heat flux (W/m^2)
Ra^* modified Rayleigh number based on the enclosure height,($g\beta q"H^4 \Pr/(\nu^2 k_f)$)
T temperature (K)
u horizontal velocity component (m/s)
U dimensionless horizontal velocity component
v vertical velocity component (m/s)
V dimensionless vertical velocity component
x horizontal coordinates (m)
X dimensionless horizontal coordinates
y vertical coordinates (m)
Y dimensionless vertical coordinates

Greek Symbols

α thermal diffusivity (m^2/s)
β coefficient of volumetric thermal expansion (K^{-1})
ν kinematic viscosity (m^2/s)
θ dimensionless temperature
φ inclination angle
ρ density (kg/m^3)
ψ stream function (m^2/s)
Ψ dimensionless stream function
ω vorticity (S^{-1})

Ω dimensionless vorticity

ΔT temperature scaling, ($q^{"} L / k_f$)

Subscripts

m average
C cold
f fluid
s source

2.MATHEMATICAL MODEL

The physical model considered here is shown in Fig. 1, along with the important geometric parameters. It consists of a rectangular enclosure of dimension, L × H, whose top wall is kept at a cold constant temperature, T_C. The aspect ratio of the enclosure is defined as A = L/H. The bottom wall has an embedded symmetrical heat source with constant heat flux, q". In general, the physical model considered here is a two dimensional rectangular enclosure and sidewalls are considered adiabatic. The Cartesian coordinates (x, y) with the corresponding velocity components (u, v) are chosen. The gravitational acceleration g acts downward normal to the x direction.

2.1 Assumptions

To simplify the problem, the following assumptions are made: the fluid is assumed to be Newtonian, steady, and incompressible. The thermophysical properties are assumed to be constant except for the density variation in the buoyancy force. The buoyancy effects upon momentum transfer are taken into account through the Boussinesq approximation. The viscous dissipation and radiation effects are considered to be negligible. The third direction of the enclosure perpendicular to the plane of the diagram is assumed to be sufficiently long so that the problem can be considered to be two dimensional. All physical properties are evaluated at the ambient temperature

2.2 Governing Equations

Once the above assumptions are employed into the governing equations for steady natural convection flow. The conservation of mass, momentum, and energy equations can be written as:

$$\frac{\partial u}{\partial x}+\frac{\partial v}{\partial y}=0.0 \tag{1}$$

$$u\frac{\partial u}{\partial x}+v\frac{\partial u}{\partial y}=-\frac{1}{\rho}\frac{\partial p}{\partial x}+\nu\left(\frac{\partial^2 u}{\partial x^2}+\frac{\partial^2 u}{\partial y^2}\right)+\beta g(\Delta T)\cos\varphi \tag{2}$$

$$u\frac{\partial v}{\partial x}+v\frac{\partial v}{\partial y}=-\frac{1}{\rho}\frac{\partial p}{\partial y}+\nu\left(\frac{\partial^2 v}{\partial x^2}+\frac{\partial^2 v}{\partial y^2}\right)+\beta g(\Delta T)\sin\varphi \tag{3}$$

$$u\frac{\partial T}{\partial x}+v\frac{\partial T}{\partial y}=\left(\frac{k_f}{\rho C_p}\right)\left(\frac{\partial^2 T}{\partial x^2}+\frac{\partial^2 T}{\partial y^2}\right) \tag{4}$$

Where, u and v are the velocity components in the x and y directions, respectively. P, T, and φ are the fluid pressure, the temperature, and the inclination angle of the enclosure with the vertical direction, respectively. ρ, β, and ν are the fluid density, the coefficient of volumetric thermal expansion, and the kinematic viscosity, respectively. ΔT, C_p, and k_f are the temperature scaling, the specific heat at constant pressure, and the thermal conductivity of the fluid, respectively.

2.3 Solution procedure

The governing equations given above, i.e., Equations (1) to (4), are given in terms of the so-called primitive variables, i.e., u, v, p, and T. The solution procedure discussed here is based on equations involving the stream function, ψ, the vorticity, ω, and the temperature, T, as variables. The stream function and vorticity are defined by:

$$u=\frac{\partial \psi}{\partial y},\ v=-\frac{\partial \psi}{\partial x},\ \omega=\left[\frac{\partial v}{\partial x}-\frac{\partial u}{\partial y}\right] \tag{5}$$

The vorticity equation is obtained by eliminating the pressure between the two momentum equations, i.e., by taking the y-derivative of Eq. (2) and subtracting from it the x-derivative of Eq. (3). Using the definition of vorticity and the continuity equation, this equation can be written as:

$$\frac{\partial \psi}{\partial y}\frac{\partial \omega}{\partial x}-\frac{\partial \psi}{\partial x}\frac{\partial \omega}{\partial y}=\nu\left(\frac{\partial^2 \omega}{\partial x^2}+\frac{\partial^2 \omega}{\partial y^2}\right)$$

$$-\beta g\left(\frac{\partial T}{\partial x}\sin\varphi-\frac{\partial T}{\partial y}\cos\varphi\right) \quad (6)$$

The equation defining the vorticity and energy equation becomes:

$$\omega=-\left[\frac{\partial^2 \psi}{\partial x^2}+\frac{\partial^2 \psi}{\partial y^2}\right] \quad (7)$$

$$\frac{\partial \psi}{\partial y}\frac{\partial T}{\partial x}-\frac{\partial \psi}{\partial x}\frac{\partial T}{\partial y}=\left(\frac{k}{\rho C_p}\right)\left(\frac{\partial^2 T}{\partial x^2}+\frac{\partial^2 T}{\partial y^2}\right) \quad (8)$$

The equations (6) to (8) are converted to dimensionless equations. By using the following dimensionless variables:

$$X=x/L,\ Y=y/L,\ \theta=(T-T_C)/\Delta T$$
$$\Psi=\psi\,\mathrm{Pr}/\nu,\ \Omega=\omega\,L^2\,\mathrm{Pr}/\nu,\ \Delta T=q^{"}L/k_f \quad (9)$$
$$Ra^{*}=g\beta q"L^4\,\mathrm{Pr}/(\nu^2\,k_f)$$

Where, X, Y, θ, Ψ, and Ω are the dimensionless horizontal coordinates, the dimensionless vertical coordinates, the dimensionless temperature, the dimensionless stream function, and the dimensionless vorticity, respectively. L, Ra^{*}, $q^{"}$, and Pr are the enclosure width, the modified Rayleigh number based on the enclosure height, the heat flux, and the Prandtl number, respectively. The dimensionless equations are:

$$\frac{\partial^2 \Omega}{\partial X^2}+\frac{\partial^2 \Omega}{\partial Y^2}=\frac{1}{\mathrm{Pr}}\left(\frac{\partial \Psi}{\partial Y}\frac{\partial \Omega}{\partial X}-\frac{\partial \Psi}{\partial X}\frac{\partial \Omega}{\partial Y}\right)+Ra\frac{\partial \theta}{\partial X} \quad (10)$$

$$\Omega=-\left[\frac{\partial^2 \Psi}{\partial X^2}+\frac{\partial^2 \Psi}{\partial Y^2}\right] \quad (11)$$

$$\frac{\partial^2 \theta}{\partial X^2}+\frac{\partial^2 \theta}{\partial Y^2}=\frac{\partial \Psi}{\partial Y}\frac{\partial \theta}{\partial X}-\frac{\partial \Psi}{\partial X}\frac{\partial \theta}{\partial Y} \quad (12)$$

Where the inclination angle, φ, is equal to 90^{O}. The appropriate boundary conditions for the governing equations are specified as follows:

Top wall: $\Psi=0,\ \theta=0\ ,\Omega=-\partial^2\Psi/\partial Y^2$

Bottom wall: $\Psi=0,\ \frac{\partial\theta}{\partial Y}=-1\ ,\Omega=-\partial^2\Psi/\partial Y^2$

Right and left walls: $\Psi=0,\ \frac{\partial\theta}{\partial X}=0,\ \Omega=-\frac{\partial^2\Psi}{\partial X^2}$

The equations (10) to (12) are converted to linear algebraic equations by substituting the corresponding approximate finite differences and then solve this set of equations by using Gauss-Siedel iterative method. The numerical method is implemented in a FORTRAN program. Typical numbers of nodal points are adopted by 37×37 uniform grid. The steady state results alone were considered when the convergence criteria defined by equation (13) are achieved.

$$\frac{\sum_{i,j}\left|\phi_{i,j}^{m}-\phi_{i,j}^{m-1}\right|}{\sum_{i,j}\left|\phi_{i,j}^{m}\right|}\le 10^{-5} \quad (13)$$

Here ϕ represents the variables θ, Ψ or Ω, the superscript m refers to the iteration number and (i , j) refers to the space coordinates. The local heat transfer coefficient, h_x, is define as $h_x=q^{"}/(T_s(x)-T_C)$ at a given point on the heat source surface where $T_s(x)$ is the local temperature along the heat source surface. Accordingly the local Nusselt number and the average Nusselt number can be obtained as:

$$Nu_x=\frac{h_x L}{k_f}=\frac{1}{\theta_s(X)} \quad (14)$$

$$Nu_m=\frac{h_m L}{k_f}=\frac{1}{L}\int_o^L\frac{1}{\theta_s(X)}dx \quad (15)$$

Where, $\theta_s(X)$, and h_m are the local

dimensionless source temperature, and the average heat transfer coefficient, respectively. The trapezoidal rule is used for numerical integration to obtain the average Nusselt number.

3.RESULTS AND DISCUSSION

Numerical simulations for different values of both the modified Rayleigh number in the range $10^3 \le Ra^* \le 10^6$ and the aspect ratio of the enclosure in the range $0.66 \le A \le 8$ are performed. The rectangular enclosure is filled with air or water. In order to point out the influence of Ra^* and A upon the flow structure type and the temperature distributions throughout the enclosure, sample local results are reported in terms of isotherms and streamlines. In all isotherm plots, the contour lines correspond to equispaced values of the dimensionless temperature θ in the range between 0 and 1 are presented. In all the streamline plots, the contour lines correspond to equispaced absolute values of the normalized dimensionless stream function are presented. Where the dimensionless stream function Ψ is defined as usual through $U = \partial\Psi/\partial Y$ and $V = -\partial\Psi/\partial X$.

3. 1 Effect of the Rayleigh number

The hydrodynamic and thermal fields in the enclosure in the form of streamlines and isotherms contour plots are represented in Fig. 2-11 for enclosure aspect ratios of 0.66, 1, 2, and 8, Rayleigh numbers of $10^4, 10^5$, and 10^6, and working fluid is air or water. The buoyancy force is acting only in the y-direction, the flow domain and boundary conditions are symmetrical and two counter-rotating rolls, and of a single cell, that remain stable as the modified Rayleigh number increasing formed in the enclosure. In addition, for $Ra^* = 10^6$ the formation of two secondary small cells near both bottom corners of the enclosure is detected. As the modified Rayleigh number and thus the buoyancy-driven circulation inside the enclosure increases, a progressive warping around the centers of rotation and a more and more pronounced compression of the isotherms toward the boundary surfaces of the enclosure do occur. The presence of the stagnation point is noticed at the midpoint of the bottom surface. The isotherm plots are also symmetrical about the vertical mid plane and concentrated towards the hot surface indicating the presence of a large temperature gradient there. The temperature gradient on the heated floor is maximum near the centre, tending to decrease toward both corners of the heat source surface. The temperature gradient is maximum near the hot wall, tending to decrease toward the cooled wall. As far as the isotherms are concerned, at $Ra^* = 10^3$ (not represented) they are very close to the typical temperature distribution that corresponds to the limit of pure conduction. For lower $Ra^* = 10^4$ the convection intensity in the enclosure is very weak as evident from the stream function values which are at least an order of magnitude smaller than those for $Ra^* = 10^5$ and 10^6. Thus viscous forces are more dominant than the buoyancy forces at lower Ra^* and diffusion is the principal mode of heat transfer. At higher Ra^* when the intensity of convection increases significantly, the core of the circulating rolls moves up and the isotherm pattern changes significantly indicating that the convection is the dominating heat transfer mechanism in the enclosure.

The effect upon the heat transfer rates is pointed out in Fig. 12, where the variation of average Nusselt number Nu_m on the heat

source surface versus the modified Rayleigh number Ra^* = 10^3- 10^6 and aspect ratio A = 2 are plotted. Besides the expected increase of the average Nusselt number on the heat source surface with the modified Rayleigh number Ra^*, the heat transfer rate from the heated floor is increased and the heat transfer rate from water is higher than that from air.

The distribution of local Nusselt number Nu_x along the heated surface versus dimensionless horizontal coordinate x/H for aspect ratio of 2 and different modified Rayleigh numbers are shown in Fig. 13 and 14 for air and water, respectively. The plots exhibit a symmetric pattern of heat transfer mechanism due to the symmetry of boundary conditions. It is to be noted that the local Nusselt number is decreased with increasing the dimensionless horizontal coordinate until half of the enclosure, after that it is increased with increasing the dimensionless horizontal coordinate. The local Nusselt number for water is higher than the local Nusselt numbers for air. The local Nusselt number is minimum at the mid-point of the heated surface.

3.2 Effect of the aspect ratio

Figure 15 shows the effect of aspect ratio in the range $0.66 \le A \le 8$ on average Nusselt numbers Nu_m of the heat source surface relevant to $Ra^* = 10^5$. The average Nusselt number Nu_m is increased with increasing aspect ratio until A=2 and then remains constant with further increase in aspect ratio. The average Nusselt number Nu_m for water is higher than that for air.

3. 3 Heat transfer correlations

Average Nusselt numbers of the heat source surface Nu_m is expressed as a function of both aspect ratio and modified Rayleigh number of enclosure through simple correlations in the following form:

For air:

$$Nu_m = 0.12\, A^{0.11}\, Ra^{*\,0.25} \qquad (16)$$

For water:

$$Nu_m = 0.14\, A^{0.12}\, Ra^{*\,0.28} \qquad (17)$$

The values of the coefficient and both exponents are evaluated by the Gauss- Seidel iteration method through a polynomial regression procedure. The correlation equations are obtained from the data in the following ranges:

$0.66 \le A \le 8$

$10^3 \le Ra^* \le 10^6$

Figures 16 and 17 represent the average Nusselt number calculated from correlations (16) and (17) versus the average Nusselt number obtained from the present simulation. It is shown from the figures that suggested equations predict the average Nusselt numbers Nu_m for air and water with maximum deviation of ±15 %.

4 Validation of the code

Furthermore, in order to validate the results of the numerical code for the present study, Fig. (18) illustrates the relationship between average Nusselt number Nu_m and modified Rayleigh number Ra^* of the present study and the results of Elif [12] for Ra^* =10^3, 10^4, 10^5, 10^6 for enclosure aspect ratio of 1, where the enclosure is filled with water. From the comparison between the two sets of results on, can observe that there is a fair agreement between them, with higher values of present results than these of Elif [12].

5. CONCLUSIONS

Natural convection in rectangular enclosures has been studied numerically, for aspect ratios A between 0.66 and 8, and for

values of modified Rayleigh number Ra^* between 10^3-10^6 for air and water. Buoyancy induced flow and heat transfer in a rectangular enclosure with localized heating through a uniform heat flux mounted at the bottom wall and uniform cold temperature at the top wall and adiabatic side walls has been numerically investigated. The main results obtained may be summarized as follows:

(i) The heat transfer rate from the heated surface of the enclosure increases as the modified Rayleigh number increases;

(ii) The heat transfer rate from heated enclosure increases as the aspect ratio increases until A=2 and then it has a constant value with further increase of aspect ratio;

(iii) The local Nusselt numbers decreases with increasing dimensionless horizontal coordinate and reaches its minimum value at x/H=1 and then increases with further increase in x/H reaching its maximum value again at x/H=2 (symmetric distribution);

(iv) Dimensionless heat transfer correlations are obtained to calculate the average Nusselt number for air and water cases.

REFERENCES

1 I. Catton, Natural convection in enclosures, in: Proceedings of the Sixth International Heat Transfer Conference, Toronto, Vol. 6, pp. 13–30, 1978.

2 S. Ostrach, Natural convection in enclosures, J. Heat Transfer Vol. 110, pp. 1175–1190, 1988.

3 M. Ciofalo, T. G. Karayiannis, Natural convection heat transfer in a partially or completely partitioned vertical rectangular enclosure, Internat. J. Heat Mass Transfer Vol. 34, pp. 167–179, 1991.

4 R. B. Chinnokotla, D. Angirasa, R. L. Mahajan, Parametric study of buoyancy-induced flow and heat transfer from L-shaped corners with asymmetrically heated surfaces, Internat. J. Heat Mass Transfer Vol. 39, pp. 851–865, 1996.

5 M. November, M. W. Nansteel, Natural convection in rectangular enclosures heated from below and cooled along one side, Internat. J. Heat Mass Transfer Vol. 30, pp. 2433–2440, 1987 .

6 A. Valencia, R. L. Frederick, Heat transfer in square cavities with partially active vertical walls, Internat. J. Heat Mass Transfer Vol. 32, pp. 1567–1574, 1989.

7 R. Anderson, G. Lauriat, The horizontal natural convection boundary layer regime in a closed cavity, in: Proceedings of the Eighth International Heat Transfer Conference, San Francisco, CA, Vol. 4, pp. 1453–1458, 1986.

8 M. M. Ganzarolli, L.F. Milanez, Natural convection in rectangular enclosures heated from below and symmetrically cooled from the sides, Internat. J. Heat Mass Transfer Vol. 38, pp. 1063–1073, 1995 .

9 O. Aydin, A. Unal, T. Ayhan, Numerical solutions for buoyancy-driven flow in a 2-D square enclosure heated from one side and cooled from above, in: Proceedings of the Advances in Computational Heat Transfer Symposium, Begell House, New York, pp. 387–394, 1997.

10 O. Aydin, A. Unal, T. Ayhan, Natural convection in rectangular enclosures heated from one side and cooled from the ceiling, Internat. J. Heat Mass Transfer Vol. 42, pp. 2345–2355, 1999.

11 A. K. A. Shati, S.G. Blakey, S.B.M. Beck, An empirical solution to turbulent natural convection and radiation heat transfer in square and rectangular enclosures, Applied Thermal Engineering Vol. 51, pp.364-370, 2013.

12 B. O. Elif, Natural convection of water-based nanofluids in an inclined enclosure with a heat source, International Journal of Thermal Sciences 48, pp. 2063–2073, 2009.

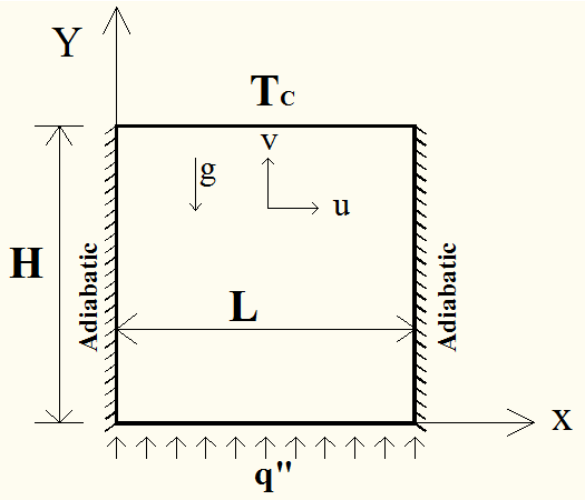

Fig. 1. Sketch of problem geometry and coordinates.

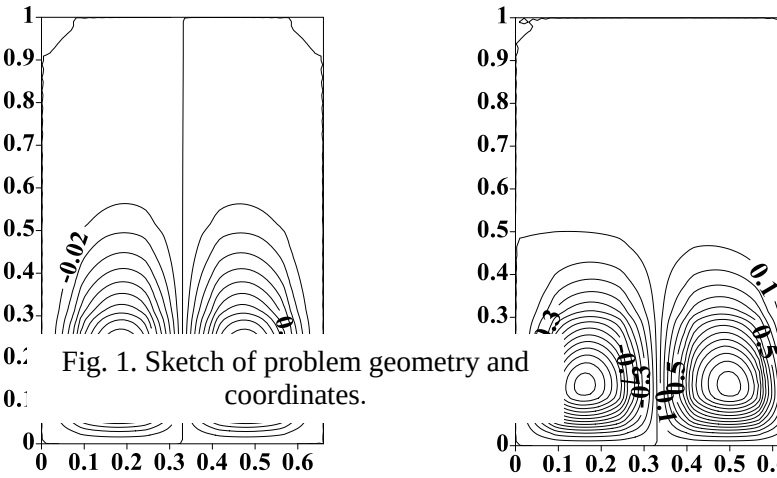

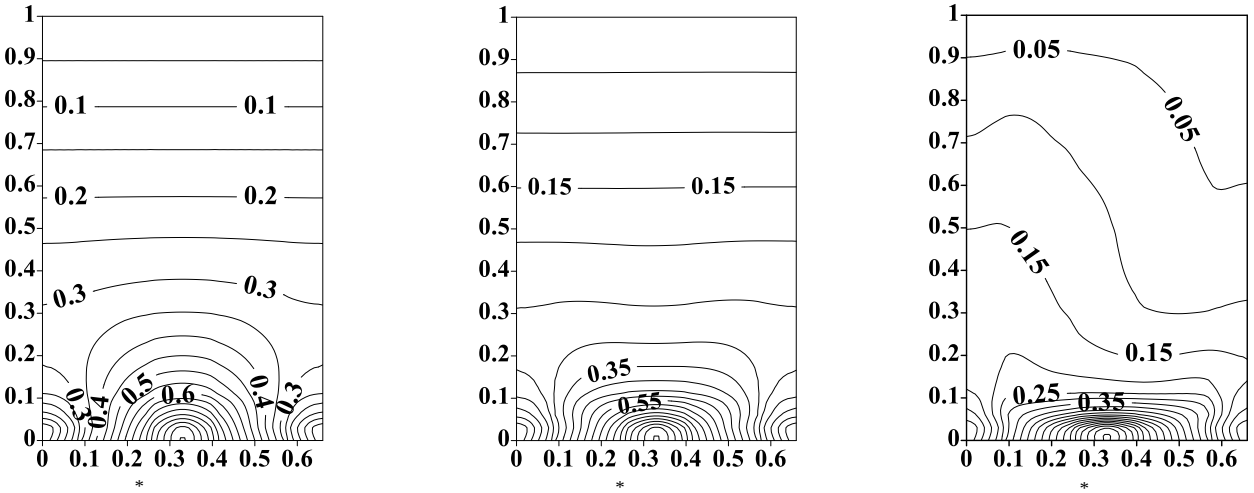

(*a*) $Ra = 10^4$ (*b*) $Ra = 10^5$ (*c*) $Ra = 10^6$

Fig. 2. Streamlines (on the top) and isotherms (on the bottom) of air at A=0.66 (L=0.66, and H=1).

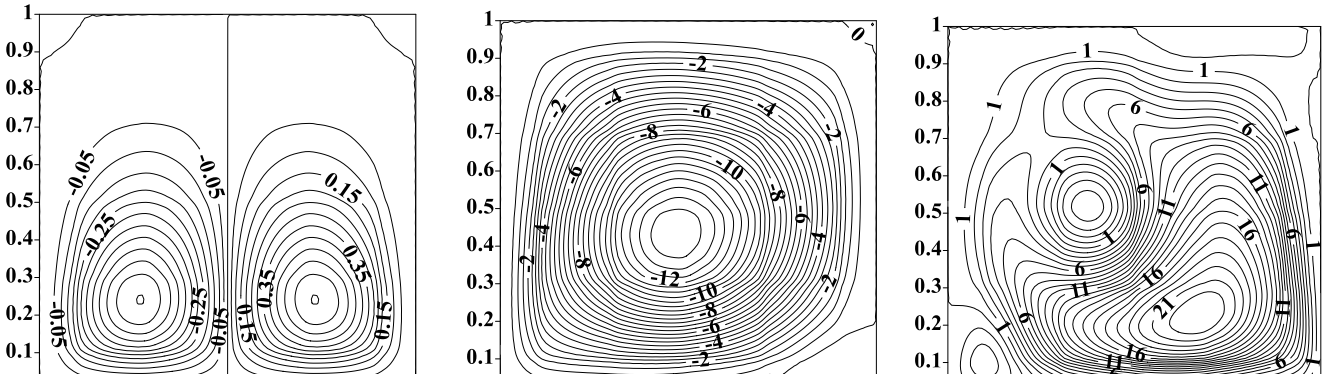

Fig. 3. Streamlines of air at A = 1 (L = 1, and H = 1).

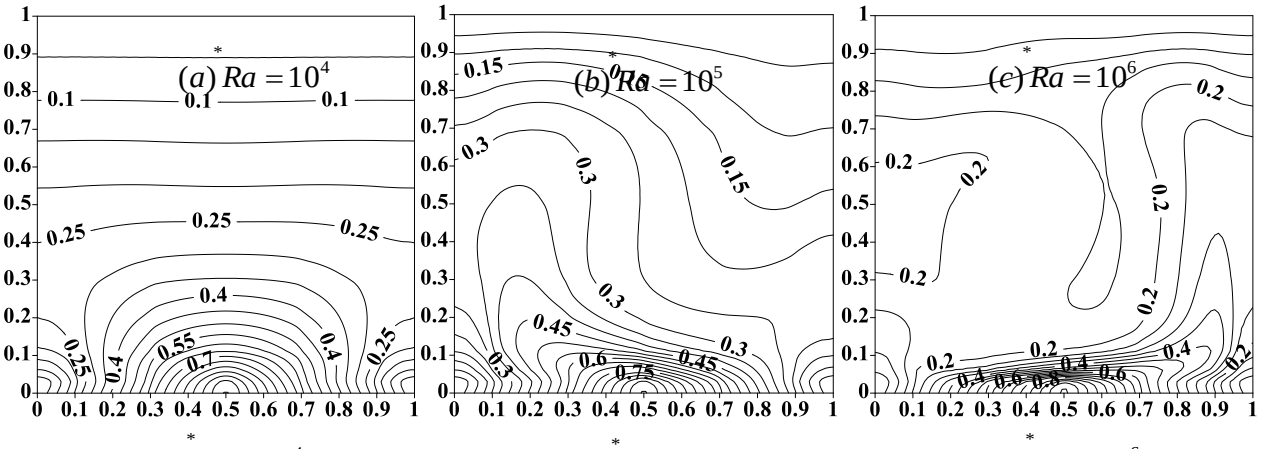

(a) $Ra = 10^4$ (b) $Ra = 10^5$ (c) $Ra = 10^6$

Fig. 4. Isotherms of air at A=1 (L=1, and H=1).

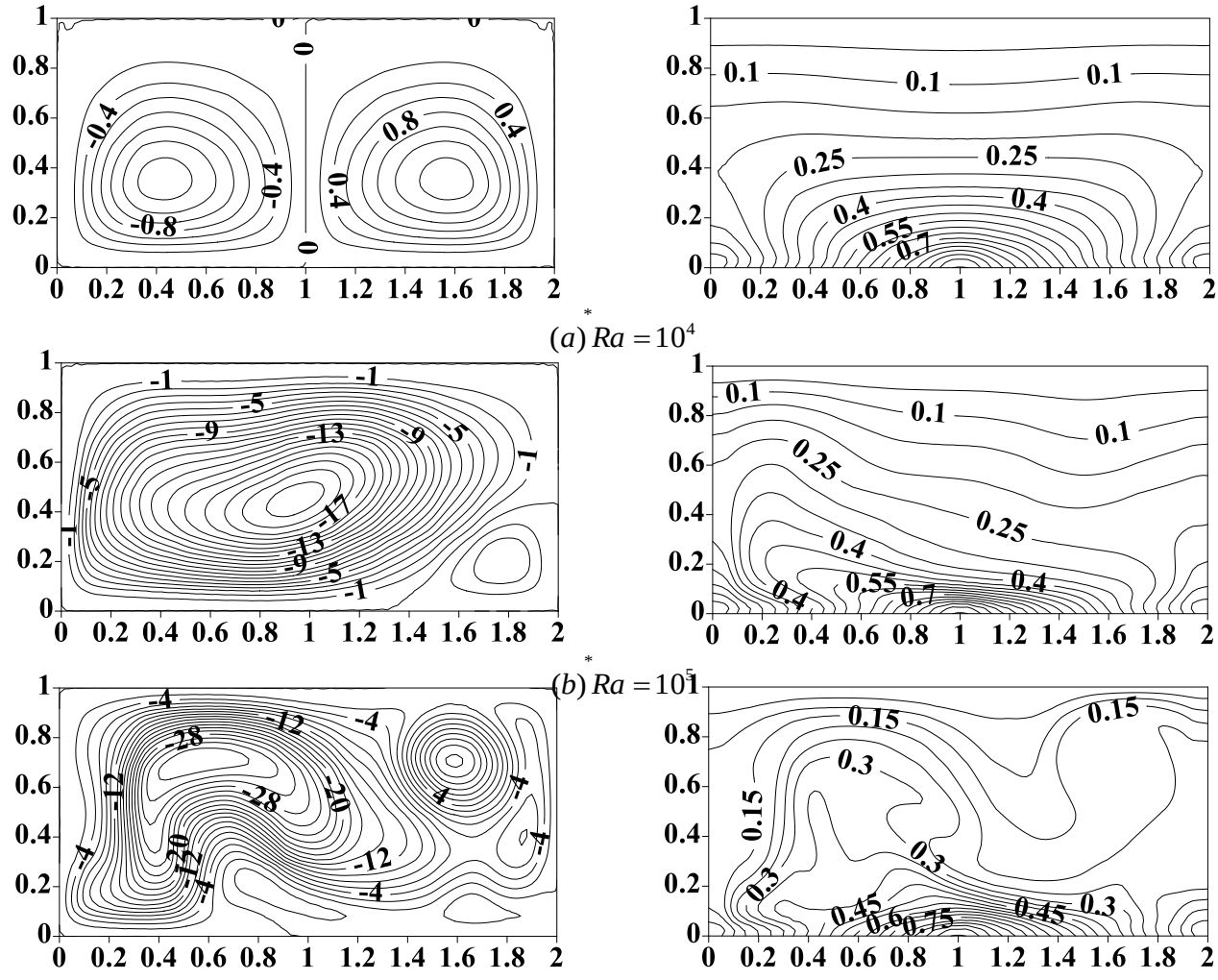

(a) $Ra = 10^4$

(b) $Ra = 10^5$

(c) $Ra^* = 10^6$

Fig. 5. Streamlines (on the left) and isotherms (on the right) of air at A=2 (L=2, and H=1).

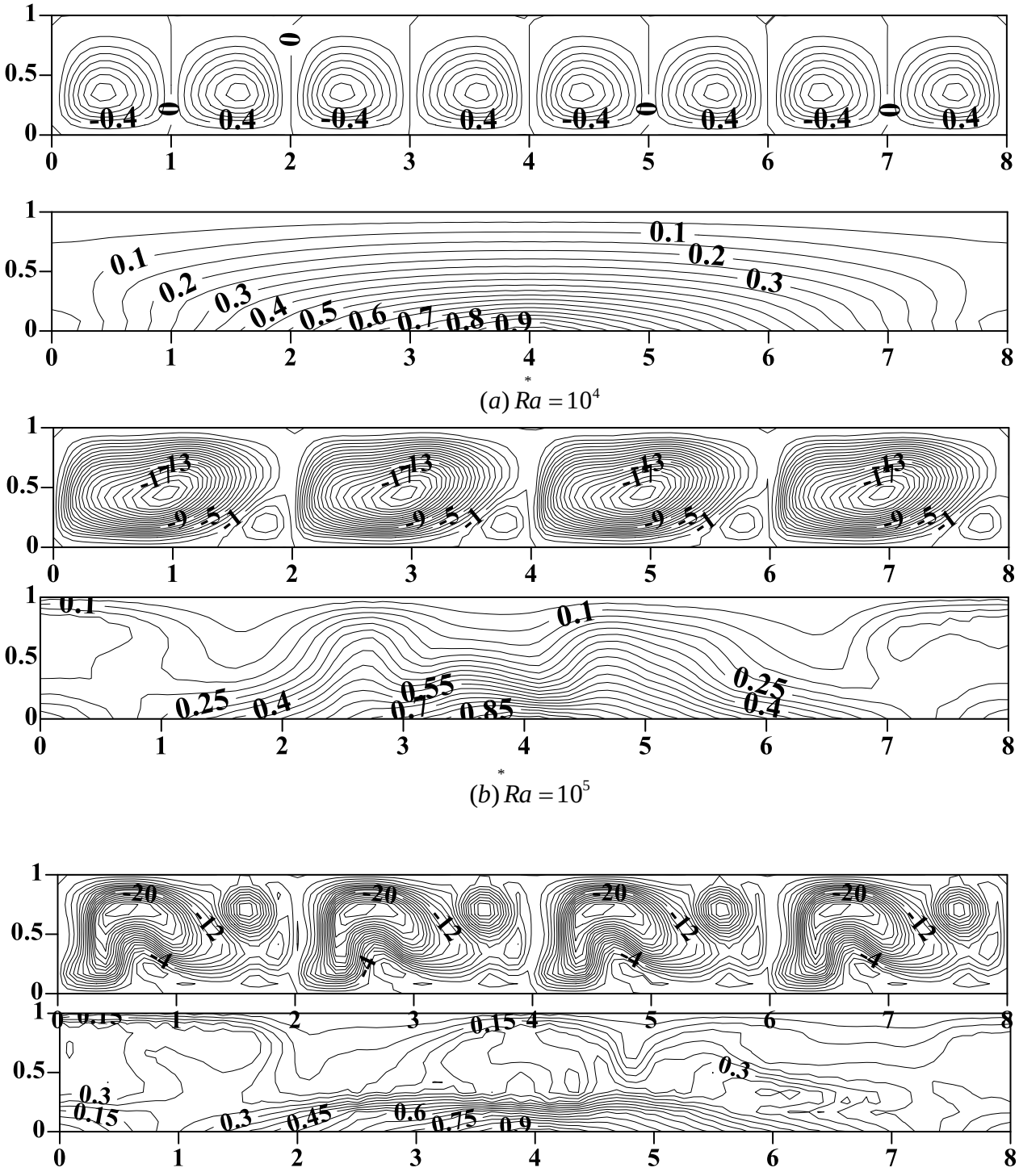

$(c)\ Ra^{*} = 10^{6}$

Fig. 6. Streamlines (on the top) and isotherms (on the bottom) of air at A=8 (L=8, and H=1).

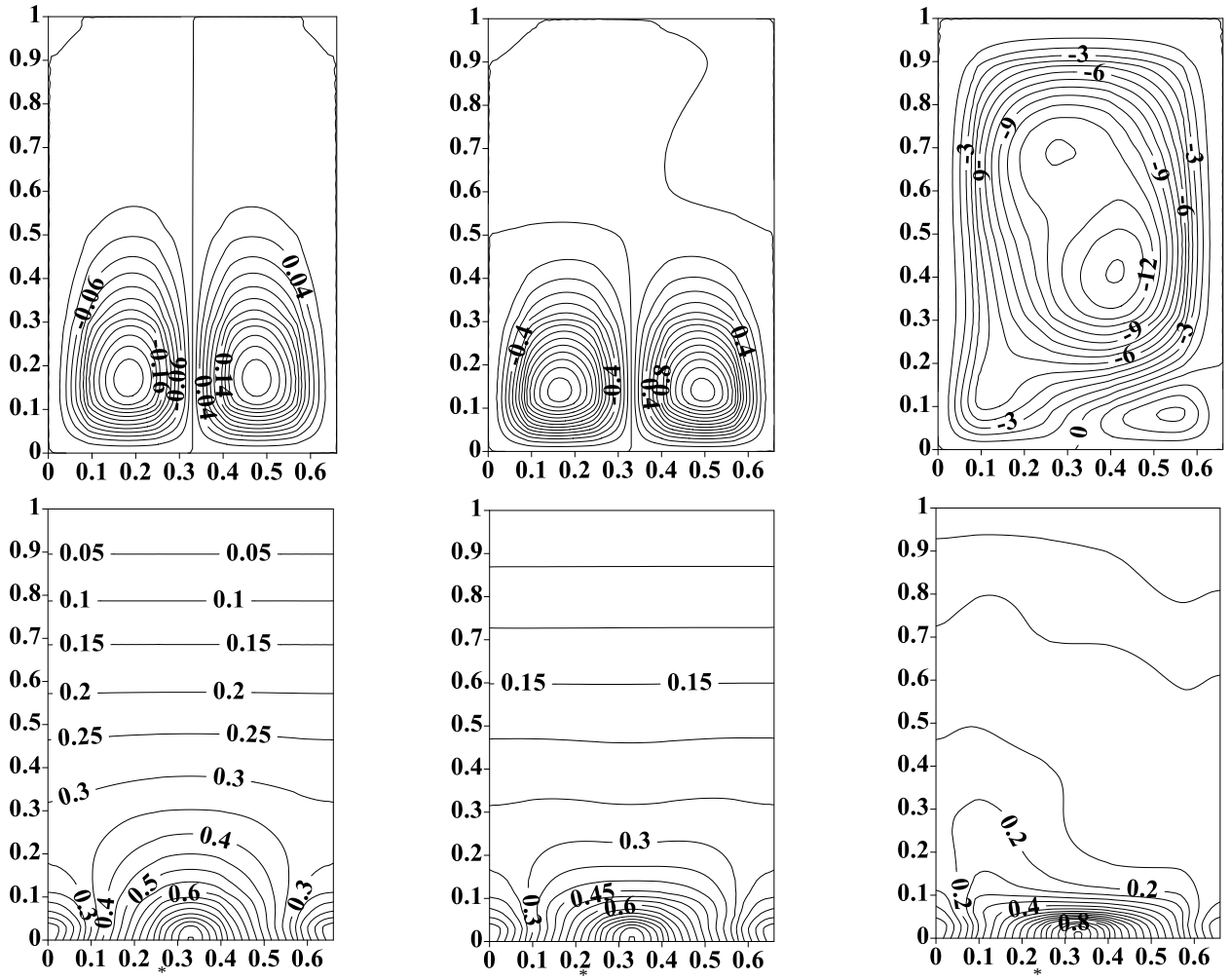

$(a)\ Ra^{*} = 10^{4}$ $(b)\ Ra^{*} = 10^{5}$ $(c)\ Ra^{*} = 10^{6}$

Fig. 7. Streamlines (on the top) and isotherms (on the bottom) of water at A=0.66 (L=0.66, and H=1).

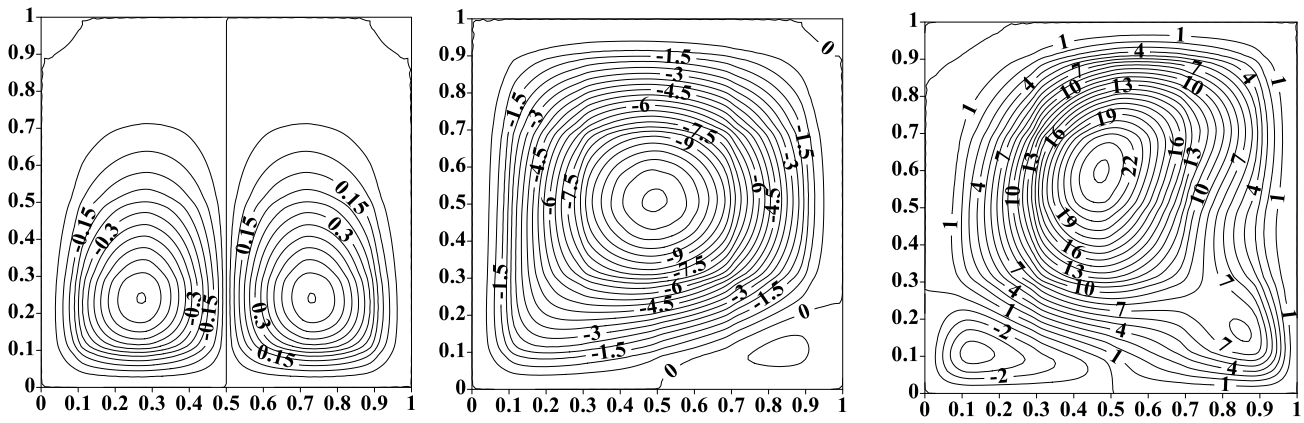

Fig. 8. Streamlines of water at A=1 (L=1, and H=1).

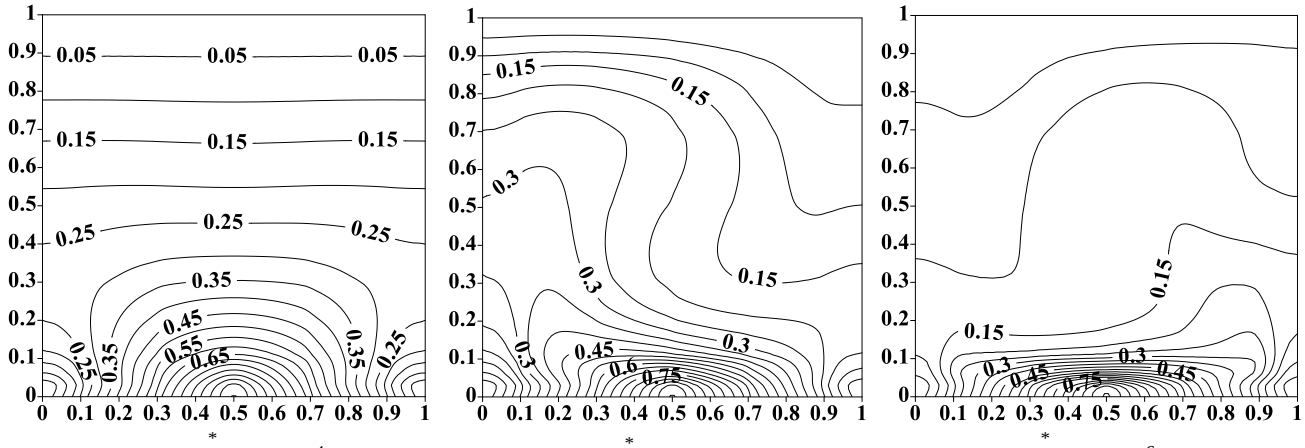

$(a)\ Ra^* = 10^4$ $(b)\ Ra^* = 10^5$ $(c)\ Ra^* = 10^6$

Fig. 9. Isotherms of water at A=1 (L=1, and H=1).

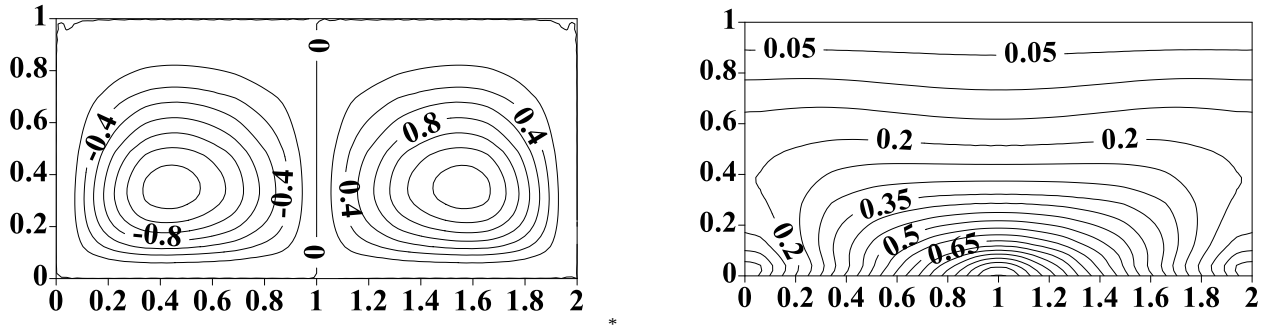

$(a)\ Ra^* = 10^4$

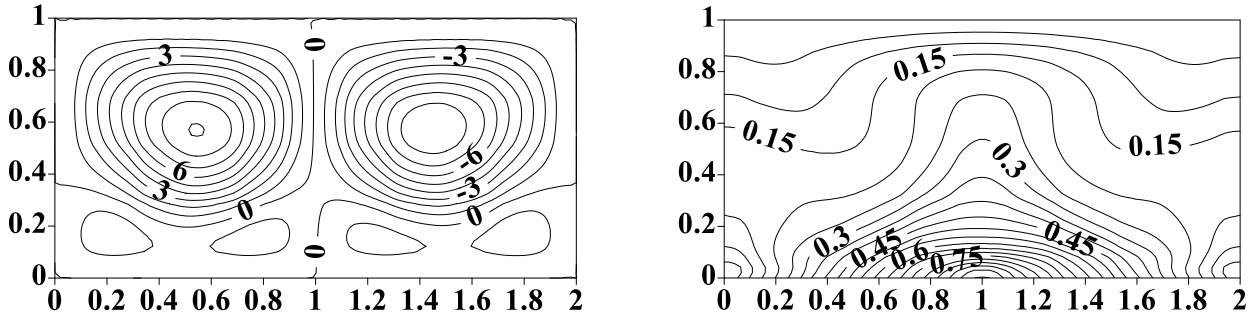

$(b)\ Ra^{*} = 10^{5}$

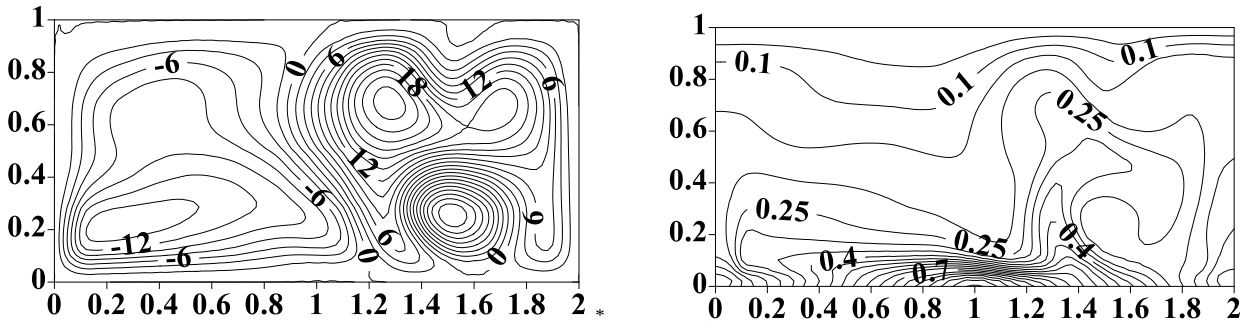

$(c)\ Ra^{*} = 10^{6}$

Fig. 10. Streamlines (on the left) and isotherms (on the right) of water at A=2 (L=2, and H=1).

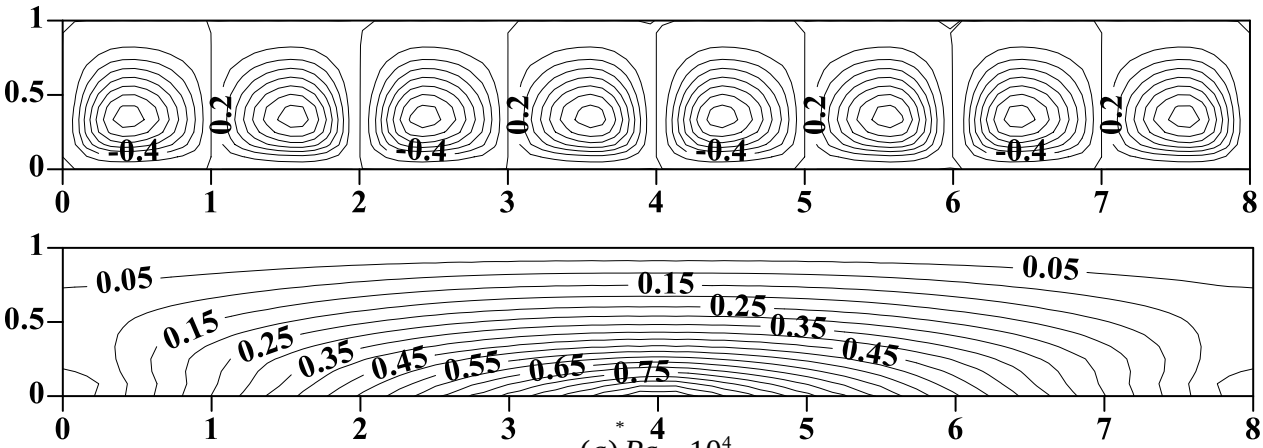

$(a)\ Ra^{*} = 10^{4}$

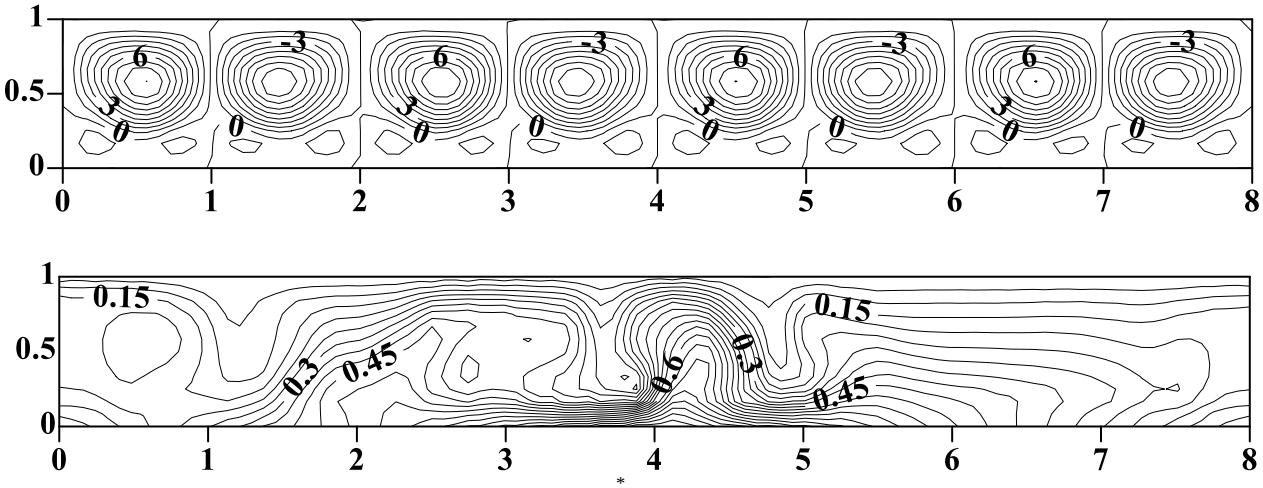

$(b)\ Ra^{*} = 10^{5}$

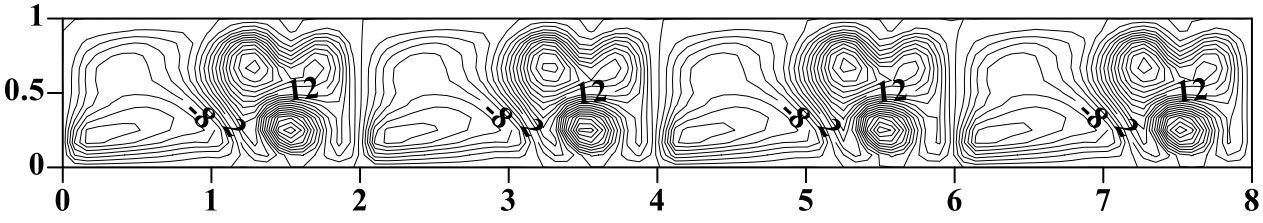

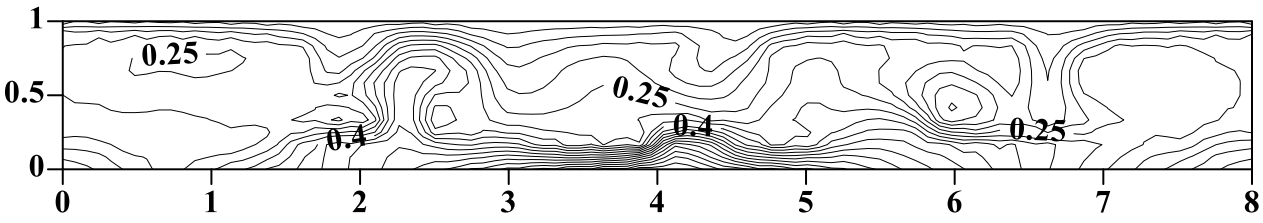

$(c)\ Ra^{*} = 10^{6}$

Fig. 11. Streamlines (on the top) and isotherms (on the bottom) of water at A=8 (L=8, and H=1).

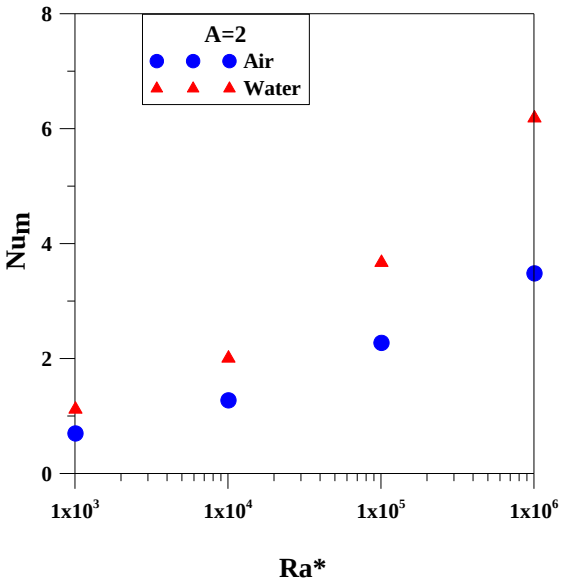

Fig. 12. Variation of Nu_m versus Ra^{*} for A = 2.

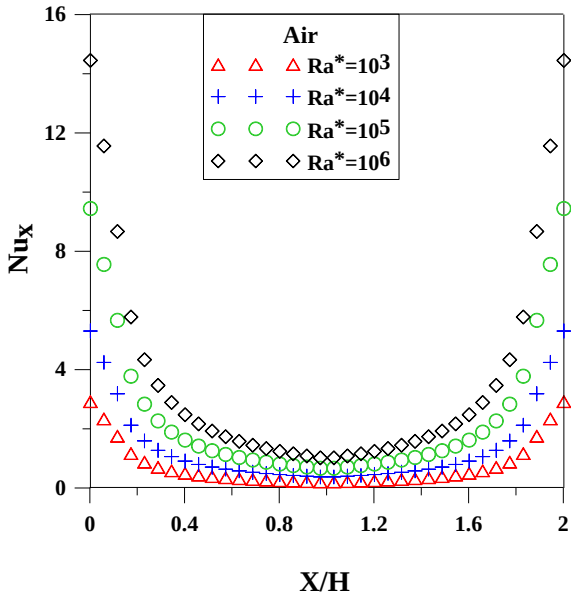

Fig. 13. Distributions of Nu_x along the heat source surface versus x/H of air for A=2.

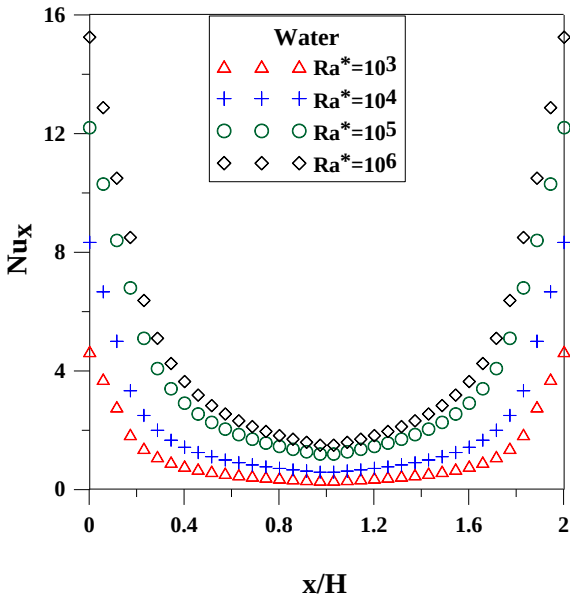

Fig. 14. Distributions of Nu_x along the heat source surface versus x/H of water for A=2.

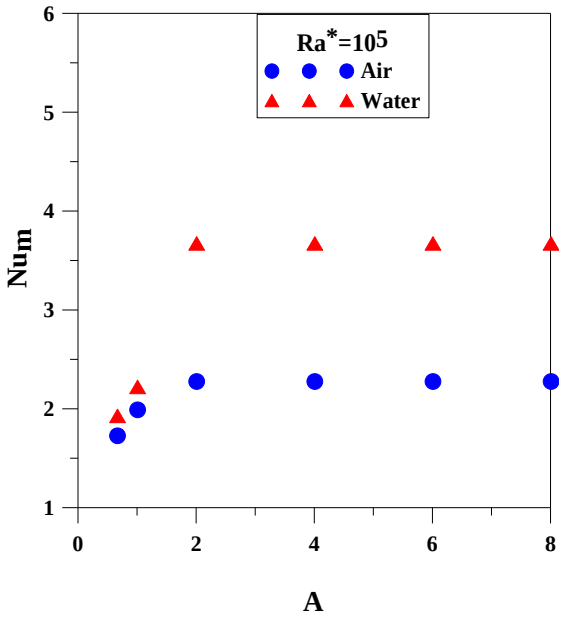

Fig. 15. Effect of aspect ratio A on Nu_m for $Ra^* = 10^5$.

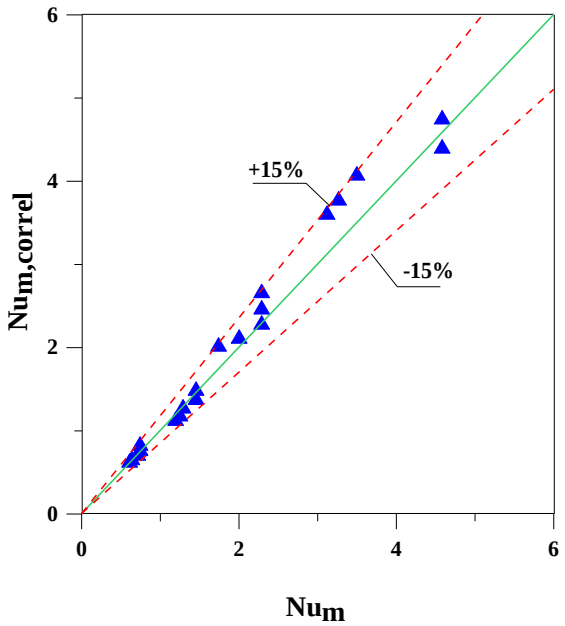

Fig. 16. Comparison between Nu_m predicted Eq. (16) and that derived from the present simulation for air filled enclosure.

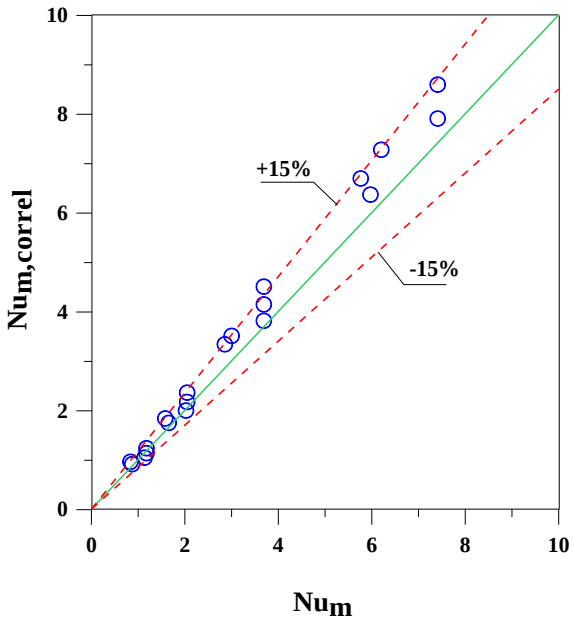

Fig. 17. Comparison between Nu_m predicted Eq. (17) and that derived from the present simulation for water filled enclosure.

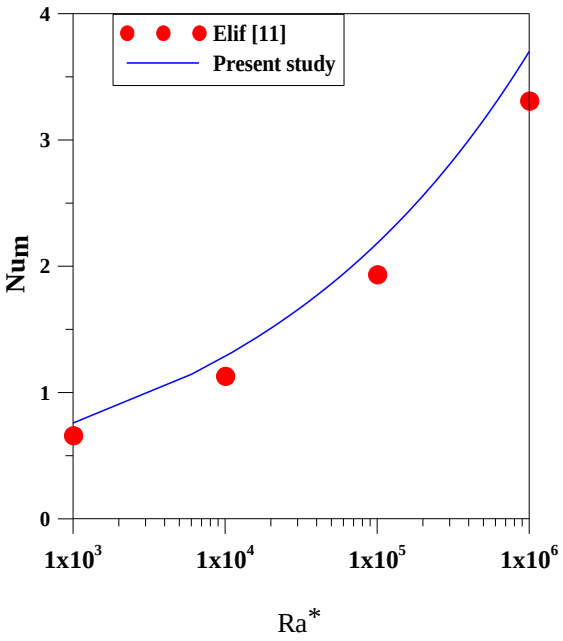

Fig. 18. Comparison between Nu_m of present study and that of Elif [12] versus $\overset{*}{Ra}$.